ICAS 2016
30th Congress of the International Council of the Aeronautical Sciences
DCC, Daejeon, Korea ; September 25-30, 2016

INFERENCE OF FLIGHT INTENT BASED ON INVERSE OPTIMAL CONTROL

Nobuhiro Yokoyama*
***National Defense Academy of Japan**

Keywords: *inference, inverse optimal control, real-time optimization*

Abstract

This paper considers a real-time inference method for the intent of aircraft. Using the observed trajectory, the proposed method solves an inverse optimal control problem based on Karush-Kuhn-Tucker optimality condition to obtain the weight of each term of the aircraft's objective function corresponding to the priority of each flight-mode. These flight-modes include direct travel to a waypoint, circling around a waypoint, avoiding regions such as severe weather areas and special use airspace, and resolving conflicts with other aircraft. The reasonableness of the inference as well as the real-time applicability of the proposed method is demonstrated through numerical examples.

1 Introduction

1.1 Backgrounds and Purpose

To enhance the safety and throughput of air traffic management, aircraft trajectory prediction plays an essential role [1]. In particular, to implement trajectory-based operations [2] in the future, the trajectory prediction is required to have a significant level of accuracy. However, the variation in aircraft's intent is one of the sources of uncertainties for both airborne and ground-based trajectory predictions [3]. The variation in intent also poses a problem when aircraft are not controlled by the centralized air traffic control system. Typical examples of this situation include operations under visual flight rules for general aviation, autonomous operations by unmanned aerial systems (UAS), and disaster relief operations involving multiple types of aircraft. While the strategic and tactical intent of each aircraft in these operations is autonomously decided by a pilot or a remote operator, or even an onboard computer, there is no effective way to share it with neighboring aircraft. With these in mind, this paper considers an inference method of aircraft intent based on the observed trajectory.

In every flight situation, an aircraft is controlled almost optimally in order to satisfy some tactical and/or strategic objective. Thus, we assume that the control input for an aircraft approximately minimizes a certain objective function and consider the inverse problem of optimal control, in other words, given a history of optimal control input during a finite period of time and a corresponding state trajectory, we estimate an unknown objective function minimized by these two factors (hereafter, 'trajectory' stands for both of these two factors). By estimating the objective function, we can infer the priority of each flight-mode. These flight-modes include traveling directly to a waypoint, circling around a waypoint, avoiding regions such as severe weather areas and special use airspaces (SUAs), and resolving conflicts with neighbor aircraft. In this way, it is possible to extract the quantified priority of the flight-modes at each sampling period.

A number of studies have examined the inference of aircraft's intent. In Ref. [4], artificial intelligence models of intent and a ranking-based algorithm for matching them was proposed. In Refs. [5-8], the residual-mean interacting multiple model (IMM) filter was used to estimate the intent and the state of an airliner. Maeder. [9] also used an IMM filter for the same purpose and predicted the future trajectory of a light aircraft based on the inferred intent. The IMM requires some difficult tuning operations, such as the tuning of the Markov

transition matrix. On the other hand, the method in the present study provides intuitively understandable inference (i.e., the priority of flight-modes at each sampling period) without the need for cumbersome tuning of parameters. Based on the inferred intent, it is possible to predict the future trajectory of the aircraft as well. Furthermore, by incorporating the inferred objective function of neighboring aircraft into the objective function of each aircraft, the proposed method also has a potential to improve the performance of the optimal control methods for conflict resolution such as the decentralized model predictive control (MPC) law [10].

The idea of the inverse optimal control has its origin in the Kalman's paper [11]. Since then, a number of studies have examined inverse optimal control, particularly as a promising approach for reinforcement learning, e.g., Refs. [12, 13]. On the other hand, to the best of the author's knowledge, there are no studies applying the inverse optimal control to flight intent inference problems except for the preliminary work by the author [14, 15]. The method adopted in the present paper represents the objective function as a weighted sum of known functions and infers the weight coefficients [16]. Johnson et al. [17] also formulated this type of problem in a continuous-time system and proposed a fast algorithm based on the linear-quadratic regulator. Nevertheless, its applications are limited to unconstrained smooth problems. Therefore, in order to accommodate a wide variety of conditions such as equality and inequality constraints and non-smooth objective functions, we formulate the discrete-time optimal control problem and apply the inference scheme based on the associated Karush-Kuhn-Tucker (KKT) optimality condition [16]. The proposed method is a modified version of that given in the preliminary work by the author [14]. It is extended to support multiple waypoints and the flight-mode to avoid regions such as severe weather areas and SUAs. The method is well suited to real-time applications because it is reduced to solving a sparse quadratic program, which is efficiently solvable and has a guarantee of convergence.

The remainder of the present paper is organized as follows. In Section 2, we introduce a dynamic model of an aircraft and then formulate the optimal control problem and its inverse, i.e., the aircraft intent inference problem. In Section 3, we show numerical examples to demonstrate the effectiveness of the proposed method. In Section 4, we summarize the findings of the present study and discuss future research.

1.2 Notation

Given n-dimensional arbitrary vectors $\boldsymbol{x}=[x_1 \ \cdots \ x_n]^T$ and $\boldsymbol{y}=[y_1 \ \cdots \ y_n]^T$, $\boldsymbol{x} \geq \boldsymbol{y}$ stands for $x_i \geq y_i$, $\forall i \in \{1,\cdots,n\}$. Given an arbitrary squared matrix $\boldsymbol{X}$, $\boldsymbol{X} \succ \boldsymbol{0}$ means $\boldsymbol{X}$ is positive definite.

2 Inference Method

2.1 Dynamic Model

For simplicity, we assume that the motion of the target aircraft (i.e., the aircraft whose intent is to be inferred) is constrained on the horizontal plane and the effect of the wind is neglected. The state equations of the aircraft as well as the enforced constraints are written as follows:

$$\begin{aligned} \dot{x} &= u \\ \dot{y} &= v \\ \dot{u} &= u\xi - v\omega \\ \dot{v} &= v\xi + u\omega \end{aligned} \tag{1}$$

$$\begin{aligned} & {V_{\min}}^2 \leq u^2 + v^2 \leq {V_{\max}}^2 \\ & (u^2+v^2)\omega^2 \leq g^2 \tan^2 \sigma_{\max} \\ & (u^2+v^2)\xi^2 \leq {a_{\max}}^2 \end{aligned} \tag{2}$$

where (x, y) is the position of the aircraft in the horizontal coordinate system, u and v are the velocities in the $x-$ and $y-$ directions, respectively, ω is the turn rate, i.e., the time-derivative of the heading angle $\tan^{-1}(v/u)$, ξ is the acceleration in the heading direction divided by the velocity, $V_{\min}$ and $V_{\max}$ are the minimum and maximum velocities, respectively, $\sigma_{\max}$ is the maximum allowable bank angle, $a_{\max}$ is the maximum allowable acceleration, and g is the gravitational acceleration.

2.2 Optimal Control Problem

2.2.1 Discretization of Time Axis

Let us discretize the time axis with time step length Δt, and let the variables with subscript k be those at each sample time $t = k\Delta t$. The state and control in this discrete-time system are defined as $\boldsymbol{x}_k := [x_k \quad y_k \quad u_k \quad v_k]^T$ and $\boldsymbol{u}_k := [\omega_k \quad \xi_k]^T$, respectively. The time domain here is defined as $[M\Delta t, N\Delta t]$, where the terminal time $N\Delta t$ corresponds to the current time, and $N - M$ is a positive constant.

2.2.2 Flight-Mode Associated with Waypoint

Let $[x_r^{(n)} \quad y_r^{(n)}]^T$ $(n = 1, \cdots, N_w)$ be the position of the reference waypoints (RWPs), which are assumed to be available via data link. In addition, let us define $\boldsymbol{\theta}_{n,k}$, $\boldsymbol{\mu}_{n,k}^+$, and $\boldsymbol{\mu}_{n,k}^-$ as follows:

$$\boldsymbol{\theta}_{n,k} = \frac{\sqrt{u_k^2 + v_k^2}\,[x_r^{(n)} - x_k \quad y_r^{(n)} - y_k]^T}{\sqrt{(x_r^{(n)} - x_k)^2 + (y_r^{(n)} - y_k)^2}} - \begin{bmatrix} u_k \\ v_k \end{bmatrix}$$

$$\boldsymbol{\mu}_{n,k}^+ = \frac{\sqrt{u_k^2 + v_k^2}\,[y_r^{(n)} - y_k \quad x_k - x_r^{(n)}]^T}{\sqrt{(x_r^{(n)} - x_k)^2 + (y_r^{(n)} - y_k)^2}} - \begin{bmatrix} u_k \\ v_k \end{bmatrix}$$

$$\boldsymbol{\mu}_{n,k}^- = \frac{\sqrt{u_k^2 + v_k^2}\,[y_k - y_r^{(n)} \quad x_r^{(n)} - x_k]^T}{\sqrt{(x_r^{(n)} - x_k)^2 + (y_r^{(n)} - y_k)^2}} - \begin{bmatrix} u_k \\ v_k \end{bmatrix}$$

The flight-mode of direct travel to the n-th RWP can be then be formulated as the minimization of $\Sigma_k\, \boldsymbol{\theta}_{n,k}{}^T \boldsymbol{\theta}_{n,k}$, because it becomes zero iff the aircraft directs its course toward the n-th RWP during the concerned period. In the same manner, the flight-mode of circling around the n-th RWP can be formulated as the minimization of $\Sigma_k\, (\boldsymbol{\mu}_{n,k}^+)^T \boldsymbol{\mu}_{n,k}^+$ (clockwise) or $\Sigma_k\, (\boldsymbol{\mu}_{n,k}^-)^T \boldsymbol{\mu}_{n,k}^-$ (counterclockwise).

2.2.3 Flight-Mode of Conflict Resolution

Let L be the number of neighboring aircraft and $r_{\min}$ be the minimum separation enforced by the flight regulation. In order to account for the flight-mode of conflict resolution with neighboring aircraft, we assume that the pilot/operator/autopilot tries to proactively make the closest distance between the own aircraft and its i-th $(i = 1, \cdots, L)$ neighbor aircraft larger than $r_{\min}$.

As shown in Fig. 1, the closest distance predicted at time $t = k\Delta t$ is calculated by the extrapolation of the relative position and velocity, where $\hat{\boldsymbol{x}}_{i,k} := [\hat{x}_{i,k} \quad \hat{y}_{i,k} \quad \hat{u}_{i,k} \quad \hat{v}_{i,k}]^T$ is the state of the i-th neighbor aircraft at time $t = k\Delta t$ and it is assumed as available. Let $\tau_{i,k}$ and $r_{i,k}$ be the time remaining to and the distance of the closest approach, respectively. They can readily be calculated as follows:

$$\tau_{i,k} = \max\left(\varepsilon, -\frac{\boldsymbol{z}_{i,k}{}^T \boldsymbol{w}_{i,k}}{\boldsymbol{w}_{i,k}{}^T \boldsymbol{w}_{i,k}}\right) \tag{3}$$

$$r_{i,k} = [\boldsymbol{z}_{i,k}{}^T (\boldsymbol{z}_{i,k} + \tau_{i,k}\, \boldsymbol{w}_{i,k})]^{1/2} \tag{4}$$

where ε is a small positive constant, and

$$\boldsymbol{z}_{i,k} := [x_k - \hat{x}_{i,k} \quad y_k - \hat{y}_{i,k}]^T$$

$$\boldsymbol{w}_{i,k} := [u_k - \hat{u}_{i,k} \quad v_k - \hat{v}_{i,k}]^T$$

As stated above, it is assumed that the conflict resolution with the i-th neighbor results from the intent to maintain

$$g(r_{i,k}, \tau_{i,k}) := \frac{\max(0, r_{\min} - r_{i,k})}{\tau_{i,k}} \tag{5}$$

be zero as far as possible for $k = M, \cdots, N$. Since $g(r_{i,k}, \tau_{i,k})$ is the maximum size of the conflict relative to the time remaining to resolve it, it represents the degree of conflict severity.

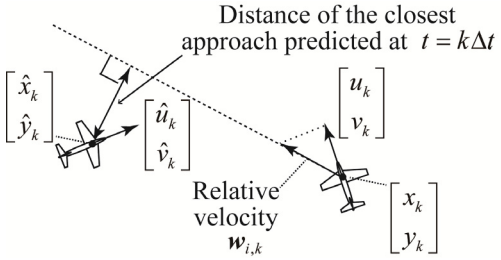

Fig. 1. Prediction of the Closest Approach

2.2.4 Flight-Mode of Avoiding Regions

In the present study, regions to be avoided such as severe weather areas and SUAs are represented by a set of N_r ellipsoids. A j-th $(j = 1, \cdots, N_r)$ ellipsoid is characterized by the center position $(\bar{x}_j, \bar{y}_j)$, the rotation angle ψ_j, and the couple of semi-major and semi-minor axes (a_j, b_j), i.e., the j-th ellipsoid is represented by

$$\boldsymbol{s}_{j,k}{}^T \boldsymbol{s}_{j,k} \le a_j b_j$$

where

$$\boldsymbol{s}_{j,k} := \frac{1}{\sqrt{a_j b_j}} \begin{bmatrix} b_j \cos\psi_j & b_j \sin\psi_j \\ -a_j \sin\psi_j & a_j \cos\psi_j \end{bmatrix} \begin{bmatrix} x_k - \bar{x}_j \\ y_k - \bar{y}_j \end{bmatrix}$$

For notational simplicity, the shape and location of ellipsoids are assumed as time-invariant, although they can readily be modified as functions of the time step k.

Let us consider a normalized space in which each ellipsoid is transformed to a circle with a radius of $(a_j b_j)^{1/2}$. Then, let $\bar{\tau}_{j,k}$ and $\bar{r}_{j,k}$ be the remaining time until the closest approach to the center of the circle in the normalized space occurs and the distance of the closest approach in the normalized space, respectively. They can be calculated as follows:

$$\bar{\tau}_{j,k} = \max\left(\varepsilon, -\frac{\boldsymbol{v}_{j,k}{}^T \boldsymbol{s}_{j,k}}{\boldsymbol{s}_{j,k}{}^T \boldsymbol{s}_{j,k}} \right)$$

$$\bar{r}_{j,k} = [\boldsymbol{s}_{j,k}{}^T (\boldsymbol{s}_{j,k} + \bar{\tau}_{j,k} \boldsymbol{v}_{j,k})]^{1/2}$$

where

$$\boldsymbol{v}_{j,k} := \frac{1}{\sqrt{a_j b_j}} \begin{bmatrix} b_j \cos\psi_j & b_j \sin\psi_j \\ -a_j \sin\psi_j & a_j \cos\psi_j \end{bmatrix} \begin{bmatrix} u_k \\ v_k \end{bmatrix}$$

In the same manner as the conflict resolution, the intent to proactively avoid each region is also modelled as an effort to maintain

$$\bar{g}(\bar{r}_{i,k}, \bar{\tau}_{i,k}) := \frac{\max(0, \sqrt{a_j b_j} - \bar{r}_{i,k})}{\bar{\tau}_{i,k}}$$

be zero as far as possible. $\bar{g}(\bar{r}_{i,k}, \bar{\tau}_{i,k})$ can be thought of as the degree of intrusion severity.

2.2.5 Formulation of the Problem

By using the variables and functions defined above, the discrete-time optimal control problem defined in the time domain $[M\Delta t, N\Delta t]$ is formulated as follows:

$$\underset{\boldsymbol{x}_M, \boldsymbol{u}_M, \cdots, \boldsymbol{x}_N, \boldsymbol{u}_N}{\text{minimize}}$$

$$\sum_{k=M+1}^{N} \sum_{n=1}^{N_w} [q_{3n-2|N} \boldsymbol{\theta}_{n,k}{}^T \boldsymbol{\theta}_{n,k} + q_{3n-1|N} (\boldsymbol{\mu}_{n,k}^-)^T \boldsymbol{\mu}_{n,k}^-]$$

$$+ \sum_{k=M+1}^{N} \sum_{n=1}^{N_w} q_{3n|N} (\boldsymbol{\mu}_{n,k}^+)^T \boldsymbol{\mu}_{n,k}^+ + \sum_{k=M}^{N} \boldsymbol{u}_k^T \operatorname{diag}(\rho_{1|N}, \rho_{2|N}) \boldsymbol{u}_k$$

$$+ \sum_{k=M+1}^{N} \left[\sum_{i=1}^{L} p_{i|N} g(r_{i,k}, \tau_{i,k})^2 + \sum_{j=1}^{N_r} \bar{p}_{j|N} \bar{g}(\bar{r}_{j,k}, \bar{\tau}_{j,k})^2 \right] \tag{6}$$

subject to

$$\boldsymbol{x}_M = \tilde{\boldsymbol{x}}_M \tag{7}$$

$$\boldsymbol{x}_k - \boldsymbol{x}_{k-1} = \frac{\Delta t}{2} [\boldsymbol{f}(\boldsymbol{x}_k, \boldsymbol{u}_k) + \boldsymbol{f}(\boldsymbol{x}_{k-1}, \boldsymbol{u}_{k-1})], \quad k = M+1, \cdots, N \tag{8}$$

$$h(\boldsymbol{x}_k, \boldsymbol{u}_k) \geq \boldsymbol{0}, \ k = M, \cdots, N \tag{9}$$

where $q_{1|N}, \cdots, q_{3N_w|N}$, $p_{1|N}, \cdots, p_{L|N}$, and $\bar{p}_{1|N}, \cdots, \bar{p}_{N_r|N}$ are nonnegative weights, $\rho_{1|N}$ and $\rho_{2|N}$ are positive weights, $\tilde{\boldsymbol{x}}_M$ is the actual state of the aircraft at time $t = M\Delta t$, and

$$\boldsymbol{f}(\boldsymbol{x}_k, \boldsymbol{u}_k) := \begin{bmatrix} u_k \\ v_k \\ u_k \xi_k - v_k \omega_k \\ v_k \xi_k + u_k \omega_k \end{bmatrix}$$

$$\boldsymbol{h}(\boldsymbol{x}_k, \boldsymbol{u}_k) := \begin{bmatrix} u_k{}^2 + v_k{}^2 - V_{\min}{}^2 \\ V_{\max}{}^2 - (u_k{}^2 + v_k{}^2) \\ g^2 \tan^2 \sigma_{\max} - (u_k{}^2 + v_k{}^2) \omega_k{}^2 \\ a_{\max}{}^2 - (u_k{}^2 + v_k{}^2) \xi_k{}^2 \end{bmatrix}$$

The quadratic term in $\boldsymbol{u}_k$ in Eq. (6) represents the cost of the control inputs. IT should be noted that Eq. (8) is derived by applying the modified Euler method to Eq. (1), and Eq. (9) is a discrete-time approximation of Eq. (2).

2.3 Inverse Optimal Control Problem

2.3.1 KKT Optimality Condition

Let the Lagrange multipliers for Eqs. (7)-(9) be as follows:

- $\boldsymbol{\eta}_{M|N} \in \mathbb{R}^4$ corresponds to Eq. (7).
- $\boldsymbol{\eta}_{M+1|N}, \cdots, \boldsymbol{\eta}_{N|N} \in \mathbb{R}^4$ correspond to Eq. (8).
- $\boldsymbol{\lambda}_{M|N}, \cdots, \boldsymbol{\lambda}_{N|N} \in \mathbb{R}^4$ correspond to Eq. (9).

Then the KKT optimality condition on the discrete-time optimal control problem given by Eqs. (6)-(9) is composed of Eqs. (7)-(9) and

$$\boldsymbol{\delta}_N = \boldsymbol{0} \tag{10}$$

$$\boldsymbol{\varepsilon}_N = \boldsymbol{0} \tag{11}$$

$$\boldsymbol{\lambda}_{k|N} \geq 0, \ k = M, \cdots, N \tag{12}$$

$$\boldsymbol{H}_N \succ \boldsymbol{0} \tag{13}$$

where $\boldsymbol{H}_N \in \mathbb{R}^{6(N-M+1) \times 6(N-M+1)}$ is the Hessian of the Lagrangian of the original optimal control problem. In addition, $\boldsymbol{\delta}_N \in \mathbb{R}^{6(N-M+1)}$ and

$\boldsymbol{\varepsilon}_N \in \mathbb{R}^{4(N-M+1)}$ denote the residuals of the stationarity condition (i.e., dual feasibility) and the complementary slackness, respectively, i.e.,

$$\begin{aligned}\boldsymbol{\delta}_N :=\ & 2\sum_{k=M}^{N}\sum_{n=1}^{N_w}[q_{3n-1|N}\boldsymbol{\theta}_{n,k}{}^T\nabla\boldsymbol{\theta}_{n,k} + q_{3n-1|N}\boldsymbol{\mu}^-_{n,k}{}^T\nabla\boldsymbol{\mu}^-_{n,k}] \\ & +2\sum_{k=M}^{N}\sum_{n=1}^{N_w} q_{3n|N}\boldsymbol{\mu}^+_{n,k}{}^T\nabla\boldsymbol{\mu}^+_{n,k} \\ & +2\sum_{k=M}^{N}\mathrm{diag}(\rho_{1|N},\rho_{2|N})\nabla\boldsymbol{u}_k \\ & +2\sum_{k=M+1}^{N}\sum_{i=1}^{L} p_{i|N}g(r_{i,k},\tau_{i,k})\nabla g(r_{i,k},\tau_{i,k}) \\ & +2\sum_{k=M+1}^{N}\sum_{i=1}^{L} \overline{p}_{i|N}\overline{g}(\overline{r}_{i,k},\overline{\tau}_{i,k})\nabla g(\overline{r}_{i,k},\overline{\tau}_{i,k})\end{aligned}$$

$$\boldsymbol{\varepsilon}_N := \begin{bmatrix} \lambda^{(1)}_{M|N}h_1(\boldsymbol{x}_M,\boldsymbol{u}_M) \\ \vdots \\ \lambda^{(1)}_{N|N}h_1(\boldsymbol{x}_N,\boldsymbol{u}_N) \\ \vdots \\ \lambda^{(4)}_{M|N}h_4(\boldsymbol{x}_M,\boldsymbol{u}_M) \\ \vdots \\ \lambda^{(4)}_{N|N}h_4(\boldsymbol{x}_N,\boldsymbol{u}_N) \end{bmatrix}$$

where $\lambda^{(i)}_{k|N}$ and $h_i(\boldsymbol{x}_k,\boldsymbol{u}_k)$ denote the i-th entries of $\boldsymbol{\lambda}_{k|N}$ and $\boldsymbol{h}_i(\boldsymbol{x}_k,\boldsymbol{u}_k)$, respectively. Moreover, the first and second derivatives are taken with respect to the concatenated vector of the variables in the original optimal control problem, i.e., $[\boldsymbol{x}_M{}^T\ \boldsymbol{u}_M{}^T\ \cdots\ \boldsymbol{x}_N{}^T\ \boldsymbol{u}_N{}^T] \in \mathbb{R}^{6(N-M+1)}$.

2.3.2 Formulation of the Inverse Problem

Let us assume that the observed trajectory of the target aircraft in the time domain $[M\Delta t, N\Delta t]$ (i.e., $[\boldsymbol{x}_M{}^T\ \boldsymbol{u}_M{}^T\ \cdots\ \boldsymbol{x}_N{}^T\ \boldsymbol{u}_N{}^T]$) is given at each time $t = N\Delta t$. Moreover, similarly to the method in Ref. [16], let us further assume that the observed trajectory is nearly-optimal to the optimal control problem given by Eqs. (6)-(9) and satisfies the above-stated KKT optimality condition in the least-squares sense. The inverse optimal control problem defined in the time domain $[M\Delta t, N\Delta t]$ can then be stated as follows:

minimize

$$\boldsymbol{\delta}_N{}^T\boldsymbol{\delta}_N + \boldsymbol{\varepsilon}_N{}^T\boldsymbol{\varepsilon}_N \tag{14}$$

subject to

$$\boldsymbol{\lambda}_{k|N} \geq 0,\ k = M,\cdots,N \tag{15}$$

$$q_{n|N} \geq 0,\quad n = 1,\cdots,3N_w \tag{16}$$

$$p_{i|N} \geq 0,\quad i = 1,\cdots,L \tag{17}$$

$$\overline{p}_{j|N} \geq 0,\quad j = 1,\cdots,N_r \tag{18}$$

$$\rho_{1|N} \geq \varepsilon,\ \rho_{2|N} \geq \varepsilon \tag{19}$$

$$\boldsymbol{H}_N \succ \boldsymbol{0} \tag{20}$$

where the decision variables are the Lagrange multipliers (i.e., $\boldsymbol{\lambda}_{M|N},\cdots,\boldsymbol{\lambda}_{N|N}$, $\boldsymbol{\eta}_{M|N},\cdots,\boldsymbol{\eta}_{N-1|N}$, and $\boldsymbol{\eta}_{N|N}$) and the weight coefficients (i.e., $q_{1|N},\cdots,q_{3N_w|N}$, $p_{1|N},\cdots,p_{L|N}$, $\overline{p}_{1|N},\cdots,\overline{p}_{N_r|N}$, $\rho_{1|N}$, and $\rho_{2|N}$). It should be noted that the residuals of the constraints of Eqs. (7)-(9) (i.e., the residuals of the primal feasibility of the KKT condition) are not functions of these variables, and hence they are independent of the inverse problem.

The above problem is a convex programming problem, because Eq. (14) is a convex quadratic form, Eqs. (15)-(19) are linear inequality, and Eq. (20) is a linear matrix inequality (LMI). However, due to the homogeneity of Eqs. (14) and (20) with respect to the decision variables, the optimal solution to the above problem is unbounded. Therefore, the following dehomogenization condition is additionally enforced:

$$\sum_{n=1}^{3N_w} q_{n|N} = 1 \tag{21}$$

Moreover, in order to assure the well-posedness, the objective function is augmented with memory terms in the following way:

$$\begin{aligned}&\boldsymbol{\delta}_N{}^T\boldsymbol{\delta}_N + \boldsymbol{\varepsilon}_N{}^T\boldsymbol{\varepsilon}_N \\ &+\sigma\left[\sum_{n=1}^{3N_w}(q_{n|N}-q_{n|N-1})^2 + \sum_{n=1}^{2}(\rho_{n|N}-\rho_{n|N-1})^2\right] \\ &+\sigma\left[\sum_{i=1}^{L}(p_{i|N}-p_{i|N-1})^2 + \sum_{j=1}^{N_r}(\overline{p}_{j|N}-\overline{p}_{j|N-1})^2\right]\end{aligned} \tag{22}$$

where σ is a positive constant. In view of the time profiles of inferred weights, the augmentation of the memory terms also has an effect of smoothing. Furthermore, in the current version of the method, Eq. (20) is eliminated. This is because Eq. (20) is a large-sized LMI which deteriorates the computational speed, although the optimization incorporating Eq. (20)

guarantees the local optimality of the observed trajectory under the calculated weights and Lagrange multipliers.

In summary, the inverse problem is to minimize the objective function given by Eq. (22) under the constraints of Eqs. (15)-(19) and (21). This problem is a convex quadratic program which has sparse patterns in the resulting matrices. Thus, it is possible to execute fast computation by off-the-shelf solvers. The weights calculated by solving this problem represent the quantified intent of the target aircraft.

3 Numerical Examples

To confirm the effectiveness of the proposed method, the numerical simulation results of three cases are shown in this section.

In each case, we firstly performed the flight simulation(s) based on the kinematic motion of aircraft. In the simulation(s), the heading vector command was given to reflect a certain intent, and the control inputs (i.e., ω and ξ) were calculated so as to follow the command as the first-order lag system with a time constant of 5.0[s]. The parameters commonly used in these simulations are shown in Table 1.

For simplicity, trajectories were assumed to be available with neither delay nor error. In addition, as mentioned above, the information on each RWP was assumed to be transmitted via data link, while the objective type (i.e., whether for direct travel or for circling) was unknown. The inference of the objective weights and the Lagrange multipliers for each aircraft was performed under the above assumptions and the following conditions: $\Delta t = 0.1$[s], $N - M = 50$, $q_{n|N-M-1} = p_{i|N-M-1} = \overline{p}_{j|N-M-1} = 0$, $\rho_{n|N-M-1} = \varepsilon$, $\varepsilon = 10^{-12}$, and $\sigma = 10^{-4}$. The sampling period of inference was specified as 1.0 [s].

Table 1. Commonly Used Parameters

Parameter	Value	Parameter	Value
$V_{\max}$	0.27[km/s]	$r_{\min}$	9.26 [km]
$V_{\min}$	0.23[km/s]	$a_{\max}$	$0.1g$ [km/ s^2]
$\sigma_{\max}$	$\pi/9$ [rad]		

3.1 Case 1: Multiple Waypoints

In this case, the trajectory of a single aircraft was simulated considering the following RWPs:

- $[x_r^{(1)} \;\; y_r^{(1)}]^T = [20.0\text{[km]} \;\; 0.0\text{[km]}]^T$
- $[x_r^{(2)} \;\; y_r^{(2)}]^T = [40.0\text{[km]} \;\; 5.0\text{[km]}]^T$
- $[x_r^{(3)} \;\; y_r^{(3)}]^T = [60.0\text{[km]} \;\; 25.0\text{[km]}]^T$
- $[x_r^{(4)} \;\; y_r^{(4)}]^T = [75.4\text{[km]} \;\; 16.6\text{[km]}]^T$

The simulated trajectory is shown in Fig. 2. Starting from $[x \;\; y]^T = [0.0\text{[km]} \;\; 0.0\text{[km]}]^T$, the aircraft firstly directed its course toward $[x_r^{(1)} \;\; y_r^{(1)}]^T$. However, it changed the course by skipping $[x_r^{(1)} \;\; y_r^{(1)}]^T$ and go directly to $[x_r^{(2)} \;\; y_r^{(2)}]^T$ at after $t = 30.0$[s]. After passing through $[x_r^{(2)} \;\; y_r^{(2)}]^T$ and $[x_r^{(3)} \;\; y_r^{(3)}]^T$, the aircraft circled around $[x_r^{(4)} \;\; y_r^{(4)}]^T$.

Figure 3 shows the inferred weights on RWP terms which were dominant during at least a certain period. Due to Eqs. (16) and (21), for $n = 1, \cdots, 4$, $q_{3n-2|N} \approx 1$ implies the inferred objective function takes the minimum when the aircraft goes directly to $[x_r^{(n)} \;\; y_r^{(n)}]^T$. In addition, $q_{11|N} \approx 1$ implies the inferred objective function takes the minimum when the aircraft circles around $[x_r^{(4)} \;\; y_r^{(4)}]^T$ counterclockwise. Thus, by comparing Fig. 2 and Fig. 3, we can confirm that each flight-mode represented by each dominant weight was consistent with the trajectory.

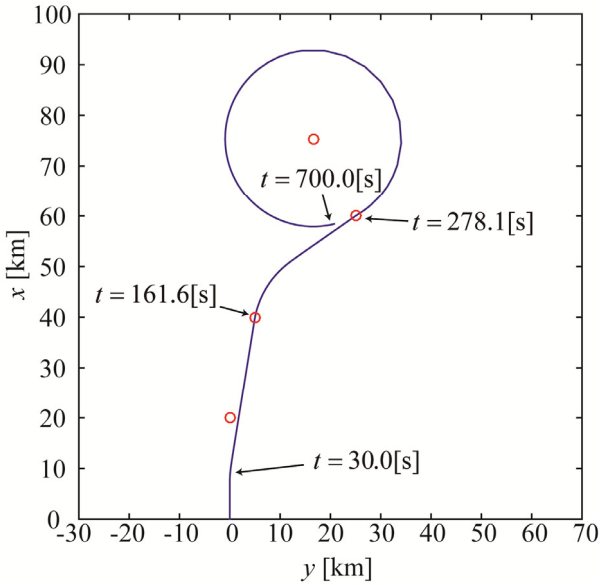

Fig. 2. Trajectory of Case 1

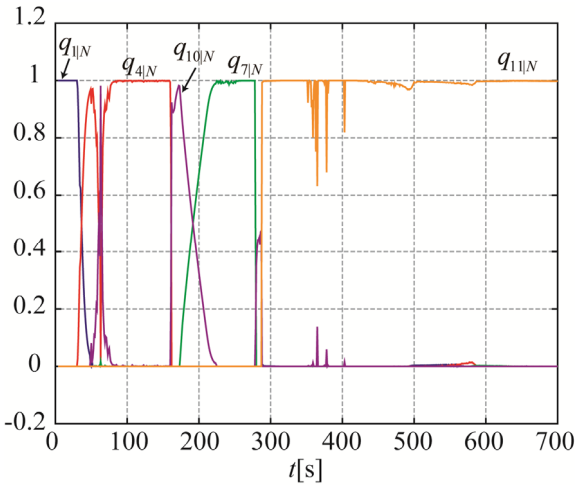

Fig. 3. Weights on RWP Terms (Case 1)

3.2 Case 2: Conflict Resolution

In this case, we simulated conflict resolution of two aircraft (referred to as aircraft A and B). Their trajectories were obtained as in Fig. 4. While the initial courses of the two aircraft were in conflict, both aircraft maneuvered rightward to resolve it. After that, they headed to individual RWPs ($[60.0[\text{km}]\ 0.0[\text{km}]]^T$ for aircraft A and $[0.0[\text{km}]\ 1.0[\text{km}]]^T$ for aircraft B). The velocity vector command for resolving the conflict was calculated by the algorithm reported in Ref. [18]. In order to consider the variation in the guidance policies, the starting time of the maneuver by aircraft A and B were specified as, respectively, 90.0[s] and 70.0[s] earlier than the predicted time of the closest point of approach (CPA). Thus, aircraft A and B started maneuver at $t = 29.7[\text{s}]$ and $t = 47.0[\text{s}]$, respectively.

Figures 5 and 6 show the inferred weights on RWP terms. As can be seen in these figures, $q_{1|N}$ (this corresponds to direct travel to the RWP) was dominant in each aircraft except for the period of large maneuver in aircraft A just after the time of CPA.

The weight on the conflict resolution term in the objective function, i.e., $p_{1|N}$, for each aircraft is shown in Fig. 7. As can be seen, the weight suddenly increased when each aircraft started maneuver to resolve the conflict. In this case, relatively large value of $p_{1|N}$, say, approximately larger than $10^{-2} \sim 10^{-3}$, seemed to correspond to the flight-mode of the conflict resolution.

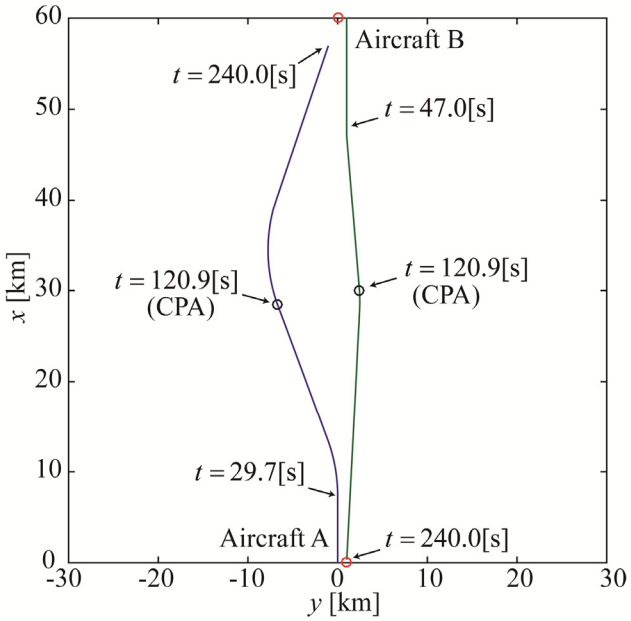

Fig. 4. Trajectories of Case 2

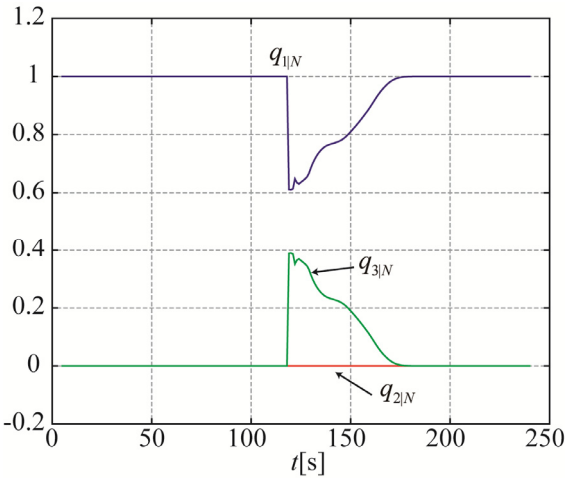

Fig. 5. Weights on RWP Terms (Case 2, Aircraft A)

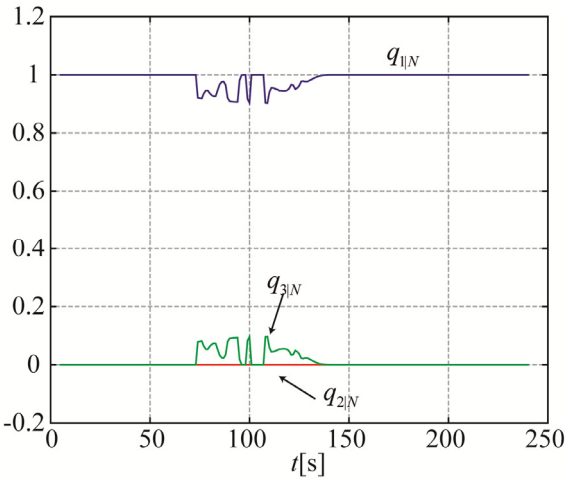

Fig. 6. Weights on RWP Terms (Case 2, Aircraft B)

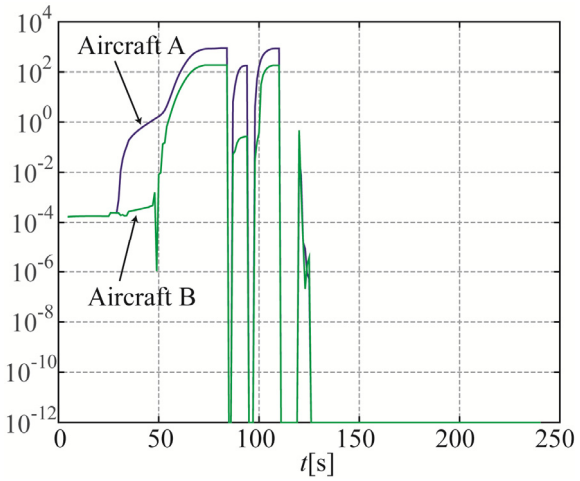

Fig. 7. Weights on Conflict Resolution Term (Case 2)

3.3 Case 3: Region Avoidance and Conflict Resolution

The region avoidance as well as the conflict resolution was simulated in this case. The trajectories of two aircraft were obtained as in Fig. 8. Similarly to the previous case, the initial courses of the two aircraft were in conflict. In addition, a region which could not be intruded was set on the initial course of aircraft A. As can be seen in Fig. 8, both aircraft maneuvered rightward to resolve the conflict, and subsequently the region was avoided by aircraft A. After that, they headed to individual RWPs ($[80.0[\mathrm{km}]\ 0.0[\mathrm{km}]]^T$ for aircraft A and $[42.0[\mathrm{km}]-40.0[\mathrm{km}]]^T$ for aircraft B). The guidance policies of the conflict resolution were the same as the previous case. Aircraft A and B started maneuver at $t=73.0[\mathrm{s}]$ and $t=86.0[\mathrm{s}]$, respectively. To avoid the region, on the other hand, a virtual waypoint was added in the vicinity of the region's boundary. Aircraft A passed through this virtual waypoint at $t=232.0[\mathrm{s}]$.

Figures 9 and 10 show the inferred weights on RWP terms. As can be seen, $q_{1|N}$ was dominant in each aircraft except for some periods of large maneuver.

The weights on the conflict resolution term and the region avoidance term in the objective function, i.e., $p_{1|N}$ and $\overline{p}_{1|N}$, for each aircraft are shown in Fig. 11 and 12. The sudden increase of the weight well corresponded to the change of the flight-mode in this case too. In addition, similarly to the previous case, if $p_{1|N}$ or $\overline{p}_{1|N}$

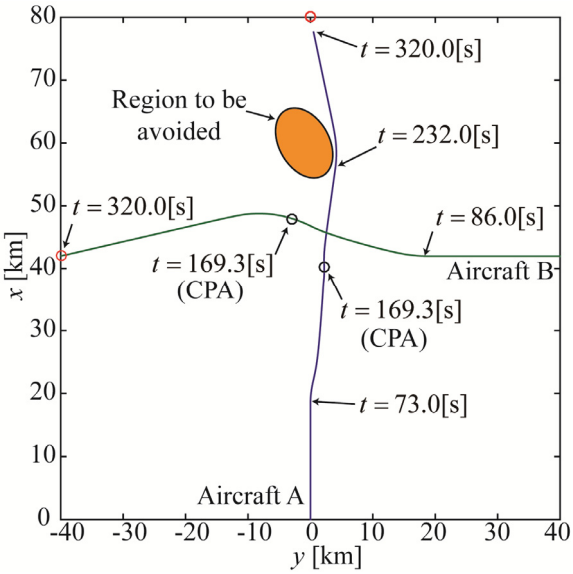

Fig. 8. Trajectories of Case 3

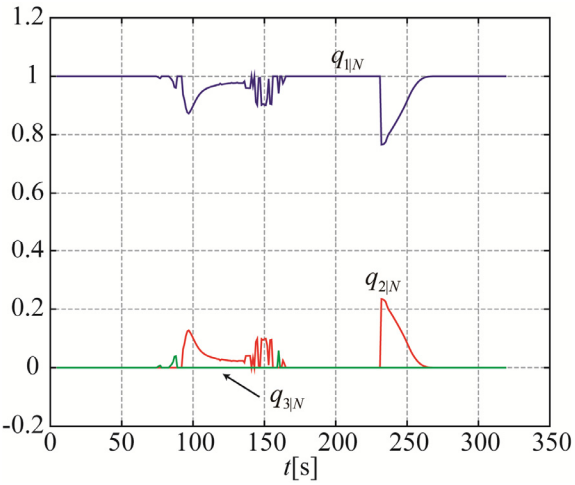

Fig. 9. Weights on RWP Terms (Case 3, Aircraft A)

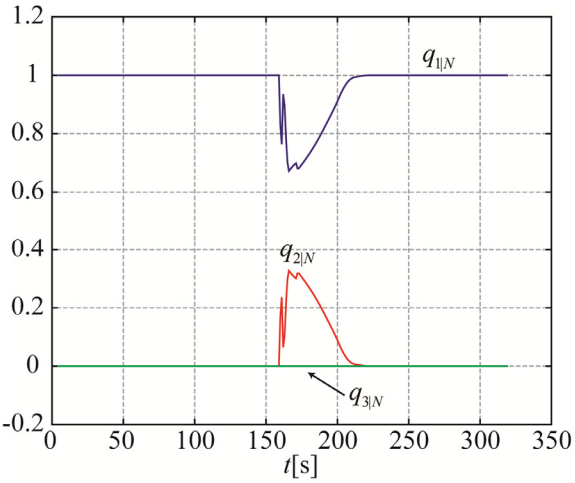

Fig. 10. Weights on RWP Terms (Case 3, Aircraft B)

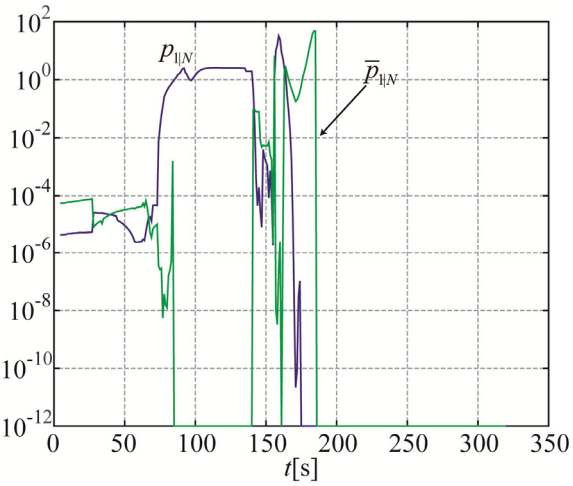

Fig. 11. Weights on Terms of Conflict Resolution and Region Avoidance (Case 3, Aircraft A)

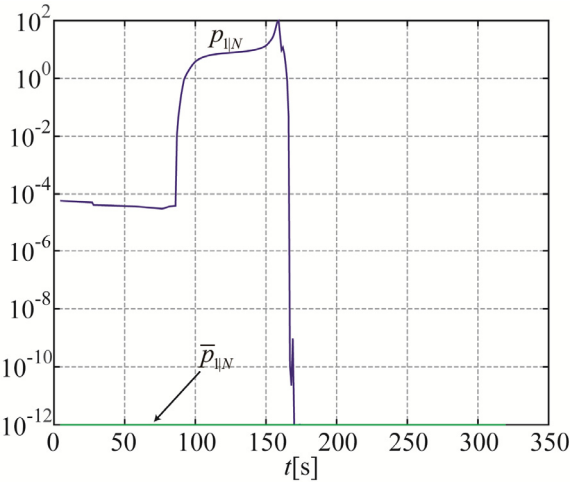

Fig. 12. Weights on Terms of Conflict Resolution and Region Avoidance (Case 3, Aircraft B)

was approximately larger than $10^{-2} \sim 10^{-3}$, it seemed to represent the flight-mode of the conflict resolution or the region avoidance.

3.4 Real-Time Applicability

For the computation in these examples, we used a laptop computer equipped with Intel® Core™ i5-3317U 1.70GHz CPU, 4.0GB RAM, and Windows 8.1 64bit OS. As the solver for the optimization problems, we employed an IBM® ILOG® CPLEX® 12.5. Table 2 summarizes the computational time per sampling period of the proposed method. Even in the worst case, the computational time was much less than the specified sampling period. This result indicates the real-time applicability of the proposed method.

Table 2. Computational Time per Sampling Period [ms]

Case	1	2		3	
Aircraft	-	A	B	A	B
Max.	297	203	187	220	235
Avg.	177	133	125	111	109

4 Conclusions

In this paper, we proposed an aircraft intent inference method based on the inverse optimal control. The proposed method infers the weights of each term of the objective function, which corresponds to the flight-mode, as well as the Lagrange multipliers by solving a sparse quadratic program at each sampling period. The inferred flight-modes include traveling directly to a waypoint, circling a waypoint, avoiding regions, and resolving conflicts with neighboring aircraft.

Through the numerical simulations, it was confirmed that the aircraft intent was appropriately quantified by the magnitude of the inferred weight of the objective function. In addition, the real-time applicability of the proposed method was also confirmed.

Directions for future work include, but are not limited to, the extension of the method to the three-dimensional space, the accommodation of wind effects, and the real-time implementation of the positive semidefiniteness condition of the Hessian to guarantee the theoretical optimality.

Acknowledgment

This work was supported by JSPS KAKENHI Grant Number 15K18289.

References

[1] Lymperopoulos I and Lygeros J. Improved multi-aircraft ground trajectory prediction for air traffic control. *Journal of Guidance, Control, and Dynamics*, Vol. 33, No. 2, pp. 347-362, 2010.

[2] Ramasamy S, Sabatini R, Gardi A G and Liu Y. Novel flight management system for real-time 4-dimensional trajectory based operations. *Proceedings of AIAA Guidance, Navigation, and Control Conference*, Boston, MA, U.S.A., AIAA 2013-4763, 2013.

[3] Zhao, Y and Zheng Q M. Modeling uncertainties in intents, guidance, and pilot actions for advanced trajectory synthesis. *Proceedings of 12th AIAA Aviation, Technology, Integration and Operations Conference*, Indianapolis, IN, U.S.A., AIAA 2012-5421, 2012.
[4] Krozel J and Andrisani D II. Intent inference with path prediction. *Journal of Guidance, Control, and Dynamics*, Vol. 29, No. 2, pp. 225-236, 2006.
[5] Hwang I, Balakrishnan H and Tomlin C. State estimation for hybrid systems: applications to aircraft tracking. *IEE Proceedings - Control Theory Applications*, vol.153, no. 5, pp. 556-566, 2006.
[6] Yepes J L, Hwang I, and Rotea M. New algorithms for aircraft intent inference and trajectory optimization. *Journal of Guidance, Control, and Dynamics*, vol. 30, no. 2, pp. 370-382, 2007.
[7] Hwang I and C. E. Seah, Intent-based probabilistic conflict detection for the next generation air transportation system. *Proceedings of the IEEE*, Vol. 96, No. 12, pp. 2040-2059, 2008.
[8] Liu W and Hwang I. Probabilistic trajectory prediction and conflict detection for air traffic control. *Journal of Guidance, Control, and Dynamics*, Vol. 34, No. 6, pp. 1779-1789, 2011.
[9] Maeder U, Morari M and Baumgartner T I. Trajectory prediction for light aircraft. *Journal of Guidance, Control, and Dynamics*, vol. 34, no. 4, pp. 1112-1119, 2011.
[10] Yokoyama N. Model predictive control for parallel planning of conflict-free trajectories for multiple aircraft. *Transactions of the Japan Society for Aeronautical and Space Sciences*, vol. 57, no. 6, pp. 352-360, 2014.
[11] Kalman, R E. When is a liner control system optimal? *Transactions of the ASME, Journal of Basic Engineering*, Vol. 86, pp. 51-60, 1964.
[12] Ng A Y and Russell S J. Algorithms for inverse reinforcement learning. *Proceedings of the 17th International Conference on Machine Learning*, San Francisco, CA, U.S.A., pp. 663-670, 2000.
[13] Abbeel P and Ng A Y. Apprenticeship learning via inverse reinforcement learning. *Proceedings of the 21st International Conference on Machine Learning*, New York, NY, U.S.A., 2004.
[14] Yokoyama N. Inference of flight mode of aircraft including conflict resolution. *Proceedings of 2016 American Control Conference*, Boston, MA, U.S.A., 2016. (to be presented).
[15] Yokoyama N. A note on flight-mode inference of aircraft. *Proceedings of the 58th Japan Joint Automatic Control Conference*, Kobe, Japan, Paper No. 1F1-4, 2015, (in Japanese).
[16] Keshavarz A, Wang Y, and Boyd S. Imputing a convex objective function. *Proceedings of 2011 IEEE International Symposium on Intelligent Control*, Denver, CO, U.S.A., pp. 613-619, 2011.
[17] Johnson M Aghasadeghi N and Bretl T. Inverse optimal control for deterministic continuous-time nonlinear systems. *Proceedings of 52nd IEEE Conference on Decision and Control*, Firenze, Italy, pp. 2906-2913, 2013.
[18] Eby M S. A self-organizational approach for resolving air traffic conflicts, *The Lincoln laboratory Journal* vol. 7, no. 2, pp. 239-254, 1994.

Contact Author Email Address

mailto:yoko@nda.ac.jp

Copyright Statement